Build Simul (2023) 16: 683–699
https://doi.org/10.1007/s12273-022-0918-8

Temporal-spatial risk assessment of COVID-19 under the influence of urban spatial environmental parameters: The case of Shenyang city

Sui Li[1,2], Zhe Li[1], Yixin Dong[3] (✉), Tiemao Shi[1,4], Shiwen Zhou[1], Yumeng Chen[1], Xun Wang[5], Feifei Qin[2]

1. School of Architecture and Planning, Shenyang Jianzhu University, Shenyang, Liaoning 110168, China
2. Institute of Ecological Urban Planning and Green Building, Shenyang Jianzhu University, Shenyang, Liaoning 110168, China
3. School of Architecture, Tianjin University, Tianjin 300072, China
4. Institute of Spatial Planning and Design, Shenyang Jianzhu University, Shenyang, Liaoning 110168, China
5. School of Science, Shenyang Jianzhu University, Shenyang, Liaoning 110168, China

Abstract

Respiratory infection is the main route for the transmission of coronavirus pneumonia, and the results have shown that the urban spatial environment significantly influences the risk of infection. Based on the Wells-Riley model of respiratory infection probability, the study determined the human respiratory-related parameters and the effective influence range; extracted urban morphological parameters, assessed the ventilation effects of different spatial environments, and, combined with population flow monitoring data, constructed a method for assessing the risk of Covid-19 respiratory infection in urban-scale grid cells. In the empirical study in Shenyang city, a severe cold region, urban morphological parameters, population size, background wind speed, and individual behavior patterns were used to calculate the distribution characteristics of temporal and spatial concomitant risks in urban areas grids under different scenarios. The results showed that the correlation between the risk of respiratory infection in urban public spaces and the above variables was significant. The exposure time had the greatest degree of influence on the probability of respiratory infection risk among the variables. At the same time, the change in human body spacing beyond 1 m had a minor influence on the risk of infection. Among the urban morphological parameters, building height had the highest correlation with the risk of infection, while building density had the lowest correlation. The actual point distribution of the epidemic in Shenyang from March to April 2022 was used to verify the evaluation results. The overlap rate between medium or higher risk areas and actual cases was 78.55%. The planning strategies for epidemic prevention and control were proposed for the spatial differentiation characteristics of different risk elements. The research results can accurately classify the risk level of urban space and provide a scientific basis for the planning response of epidemic prevention and control and the safety of public activities.

Keywords

COVID-19;
virus infection rate;
GIS data simulations;
urban morphological parameters analysis;
infection risk assessment;
epidemic containment planning

Article History

Received: 10 April 2022
Revised: 07 June 2022
Accepted: 25 June 2022

1 Introduction

The COVID-19 pandemic has had an unprecedented impact on human health and public safety. Up to today, since the virus is widely spread around the world, under the situation of a normalized epidemic, effective prevention strategies for urban public spaces are an important influencing factor to maintain urban safety and promote economic recovery. As outdoor spaces for daily life and social activities of urban citizens (Wu and Li 2011), urban public spaces are the central place for human contact and communication and also serve as an essential source for urban vitality (Jacobs 1964; Tibbalds 1992). However, with the highly populated complex environment, urban public spaces are critical for respiratory infectious disease prevention and control. Carrying out the multidimensional dynamic evaluation on

E-mail: dongyixin@tju.edu.cn

the risk of COVID-19 respiratory infection in urban space and accurately classifying the risk level of urban spaces are the premises for scientific prevention and critical control of the epidemic (Li et al. 2020).

Nowadays, many countries have established information platforms on the dynamics of the Covid-19 epidemic[1] and carried out risk-area ranking. Platform information is mainly used to monitor case occurrence locations and patient activity trajectories (Kamel Boulos and Geraghty 2020; Zachreson et al. 2021), intercity population movement (Peixoto et al. 2020; Jiang et al. 2021), health care resource allocation distribution (Kang et al. 2020; Sha et al. 2020), etc. For the classification of risk areas, urban administrations are more likely to classify the risk levels of different administrative areas based on epidemiological surveys, the number of existing infection cases, and the clearance interval. In contrast, in some research work, the classification of urban risk zones is more considered to introduce more influencing factors, and the spatial scale of the classification is more detailed.

Taking Eswatini in Africa as an example, Dlamini et al. (2020) formulated the COVID-19 comprehensive risk evaluation map in three risk levels based on the national dimension with multivariate clustering method on the basis of the annual average traffic volume, case report position and ward number in hospitals. They explored the possibility of prediction of the spatial risks for the epidemic with the shortage of the statistical data on the cases and the limited medical and healthcare capacity. Azevedo et al. (2020) formulated the risk evaluation map in the national dimension in urban spaces based on the geological model of block sequential simulation according to the confirmed case number reported every day in Portugal. They optimized the infection risk evaluation tolerance resulting from the difference of the urban population scale without considering the risk classification of traditional choropleth map. Wang et al. (2020) based on the epidemic cases and POI data in Shaanxi Province, China, used mathematical statistics, spatial analysis and other methods to identify the hot risky zones in the downtown dimension by making the geographic profiling for the street risk indexes in the urban area of Xi'an city through the overlay assignment for density grid in the epidemic communities, crowd gathering point and the designated medical institution. These related researches around the spatial distribution of the risk of Covid-19 epidemic make up for the deficiencies of traditional epidemic risk zone delineation in terms of spatial accuracy. Generally, they show the following development trends. (1) Introducing information on the urban environment and human flow characteristics for risk assessment and improving spatial delineation accuracy is applicable to control during severe epidemic outbreaks and can guide citizens' behavior guidance during the epidemic normalization period. (2) Evaluation results focus on the combination of immediacy and dynamism, with the function of extrapolation and prediction of epidemic risk under various scenarios.

In addition, some countries also specify the division of spatio-temporal concomitant risk of the new coronavirus. In China, for example, the conditions for spatio-temporal concomitant risk are co-existence for 10 minutes or accumulation of more than 30 hours on either side in an 800 m × 800 m grid. The latter is applicable in indoor spaces such as homes and offices in terms of exposure time. At the same time, the former is more applicable to spatio-temporal intersections arising from the flow of people in public open spaces. This paper focuses on the former, i.e., the assessment of respiratory infection risk in urban public spaces due to spatio-temporal intersections arising from the flow of people. Moreover, it proposes a method to accurately evaluate the Covid-19 epidemic in urban public spaces based on the combination of the urban built environment and spatial distribution of the population. We propose a method to accurately evaluate the risk of a Covid-19 epidemic in urban public space based on the combination of the urban built environment and spatial distribution of the population. It can be used as an in-depth discussion of the current method to classify spatio-temporal concomitant risks in epidemic prevention and control.

WHO (2020) report has shown that COVID-19 goes along with the transmission modes and infection mechanism of airborne infectious diseases. The respiratory infection probability model is commonly used to evaluate the risk of airborne infectious diseases such as COVID-19. The Wells-Riley (W-R) model was proposed by Wells (1955) with the "quanta" concept and was finally developed and formulated by Riley et al. (1978) on this basis. Afterward, this model was widely used to evaluate infection risks in crowded spaces, such as hospital wards, public transport means, and prisons (Noakes et al. 2006; Zhu et al. 2012; Urrego et al. 2015). This model was initially used under the premise of uniform distribution of virus concentration in space and could not reflect the spatial heterogeneity of infection risks resulting from the flow field difference under different environments (Furuya 2007; Chen and Liao 2008). With the progress of the studies, some scholars shifted the perspectives from the single space environment to the complex space environment influenced by multiple factors. Qian et al. (2009) built a new mathematical model for predicting the spatial distribution of infection risks for airborne diseases by combining the Wells-Riley equation with the computational fluid dynamics model and analyzing

1 For example, https://ncov.dxy.cn/ncovh5/view/en_pneumonia; https://coronavirus.data.gov.uk; https://www.mhlw.go.jp/english/

and evaluating the difference of the infection risks in different zones of the wards during the large-scale outbreak of SARS in HK hospitals in 2003. Noakes and Sleigh (2008) combined Wells-Riley equation with the mixed ventilation equation, for simulative calculation of infection risks of respiratory diseases for 18 patients in three wards connected by a corridor, finding that the number of newly infected patients in different communities has different growth curve over time, and being nearer to the source of infection indicates higher risk level. Based on the W-R model, this study explored the spatial heterogeneity of infection risks for respiratory diseases after considering the factors imposed upon the environment, such as flow field difference, and has provided a theoretical basis and method for our study.

This study explored the important parameters for human body respiration and effective scope of influence in W-R model through the literature combing, made the respiratory infection risk evaluation in the grid cell with the local environmental monitoring data, inferred this method to the urban dimension, and strived to seek the space path and planning response strategy in atmospheric protection by formulating the accurate classification of the infection risk level in urban public spaces.

2 Modeling

This study has proposed the framework for infection risk assessment of infectious respiratory diseases in urban public spaces (in Figure 1), We divided the study area into 100 m × 100 m grids, and achieved quantitative evaluation of respiratory infection risk in urban public space by coupling the results of human flow and local wind environment assessment within the grids.

2.1 Module 1: W-R formula extension based on the scope of individual respiratory influence

Based on the Wells-Riley model for classical risk assessment of respiratory diseases, the calculation formula is as follows:

$$P = \frac{C}{S} = 1 - \exp\left(\frac{-Iqpt}{Q}\right) \quad (1)$$

where, P is the infection probability, C is the number of newly infected persons, S is the total number of susceptible persons. I is the number of infected persons. In this study, the research zone is divided into 100 m × 100 m grids, where the initial value for the number I of the newly infected

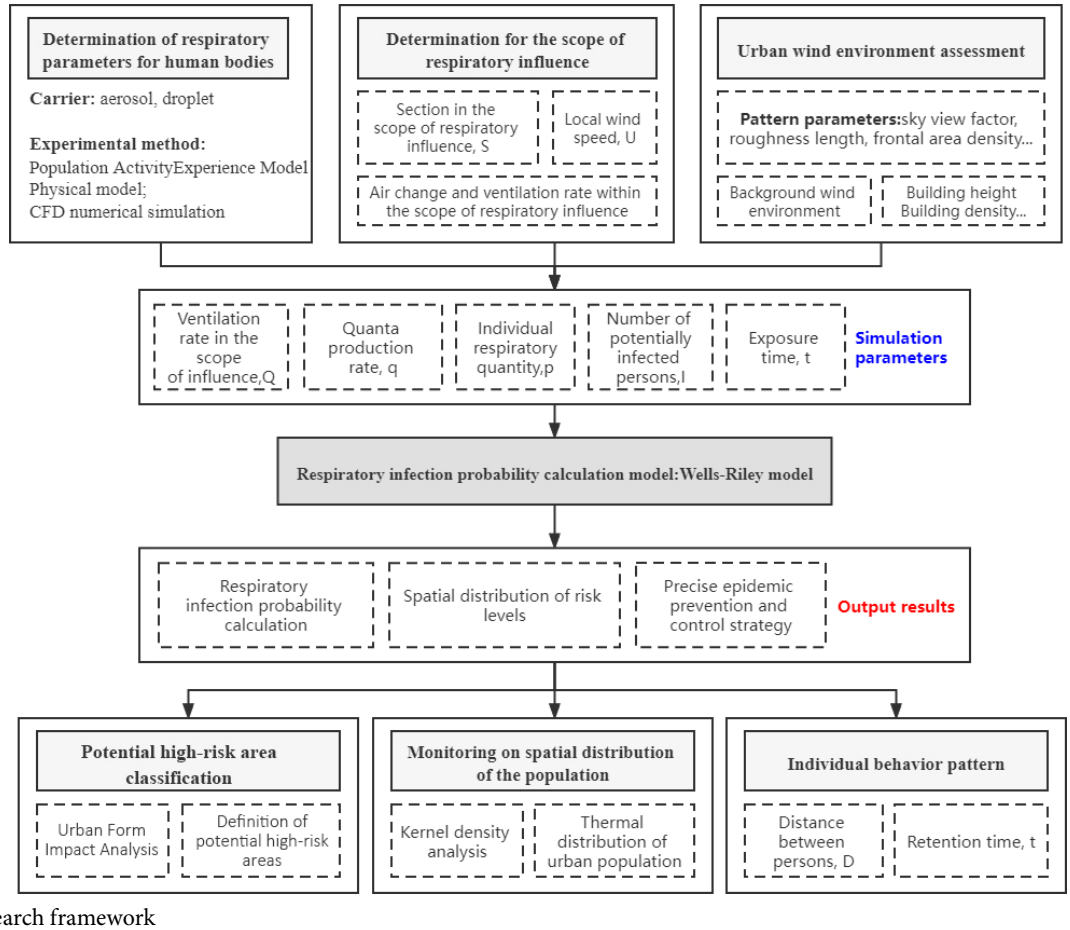

Fig. 1 Research framework

persons in the grid cell is set to 1, followed by the statistics of the mean value of the number of persons in different time segments for the grid cell, taking its logarithmic function for the weighting of the initial value, as the number of potentially infected persons in this grid. q is the quanta production rate of an infected person, and the currently available research result is adopted in this study (Buonanno et al. 2020; Dai and Zhao 2020; Zhang et al. 2020), taken as 122 quanta/h. p is the ventilation rate for respiration by the individual (m^3/h), referring to the related respiratory tract infectious disease parameters (Qian et al. 2012), taken as 0.6 m^3/h. t is the exposure time (h), and is discussed as a variable in multiple scenarios. Q is the ventilation rate of the local space (m^3/h), and its determination basis will be discussed below.

W-R model is based on the presupposition for a particular value of quanta. It is supposed with uniform distribution of virus concentration in the scope of the space under the research, so it is not required to consider the spatial position of the patients being the source of infection. However, current studies have found that air currents in the actual urban environment lead to a non-uniform distribution of the viral concentration. The spatial location of the infectious source and the dilution of the exhaled air are closely related to the risk of infection in the surrounding area. Therefore, the discussion of the range of human respiratory impact and the risk of virus infection has become a hot topic of research in related fields in recent years (Gralton et al. 2011; Villafruela et al. 2013; Xu et al. 2017). As shown in Table 1, this study combed the related data regarding the scope of respiratory influence in recent years, which has been used as the basis for determination of Q, the ventilation rate of local space in a specific environment, and improved the original W-R model.

The current study proves (Table 1) that as the distance between people increases, the effective respiratory segment area increases accordingly. There is a definite relationship between them when the virus concentration gradually decreases with the increase in the distance between the test point and the infected source. At the same time, the researchers found that the wind environment in the space can have a drastic effect on the trajectory of the droplets exhaled by the infected person, which in turn affects the virus concentration. Therefore, to determine Q, both of these influencing factors should be considered (Figure 2), i.e., the spatial scale within the influence of the infected person's breath and the instantaneous ventilation under the influence of the vector wind speed (U_i). The W-R equation is extended as follows:

$$P = 1 - \exp\left(\frac{-Iqptk}{Q}\right) = 1 - \exp\left(\frac{-Iqptk}{SU_i}\right) \quad (2)$$

$$S = H \times L = f(D) \times L \quad (3)$$

where, U_i is the local wind speed in different environments, which is determined after calculation with Module 2; k is the virus filtration factor for personnel wearing masks (values taken in this paper are 0.5 and 0.95); S is the section area for effective influence by the respiration of the infected person, referring to Table 1, expressed as $H \times L$, where the height H, is the function of the distance between persons D, expressed as $H = f(D)$.

2.2 Module 2: ventilation environment and local wind speed assessment of grid cell

This study quantifies the local surface ventilation environment for different grids by extracting urban morphology parameters in the grid cell. It then infers the local wind speed by simulating with the urban background wind speed. The ventilation environment of the grid cell is estimated by using the dynamic roughness length (RL) of the underlying surface and sky view factor (SVF) (Liu et al. 2019). Roughness length is a crucial parameter influencing the local wind environment, and the research methods include meteorological observation (Grimmond 1998; Gualtieri and Secci 2011) and model calculation (Borak et al. 2005; Chen et al. 2010). This study uses the urban completed

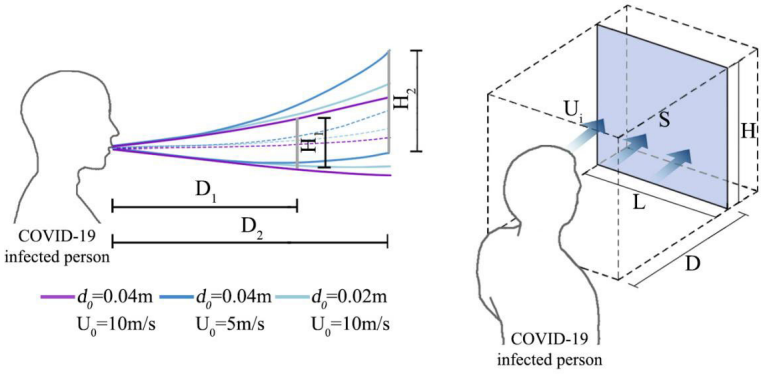

Fig. 2 Sketch map of the scope of effective influence of the droplets of the infected persons (Xie et al. 2007; Liu et al. 2017)

Table 1 Determination basis for the scope of effective influence by the respiration of the infected persons in urban public space

Reference	Research content and method	Main parameter values for the scope of influence by the respiration of human body dimension
Xie et al. 2007	Study the evaporation and movement of the droplets expelled during respiratory movement through the calculation with the physical model, and explore the basic transmission mechanisms of infectious diseases.	The droplet jet trajectory is related to the initial jet velocity and the mouth-opening size. At the horizontal distance of 1m, the vertical influencing distance is about 0.5m, and at the horizontal distance of 2m, the vertical influencing distance is about 1m. The horizontal influencing distance of droplets generated by sneezing (50m/s) is greater than 6m, the horizontal influencing distance generated by coughing (10m/s) is greater than 2m, and the horizontal influencing distance generated by breathing (1m/s) is within 1m.
Liu et al. 2017	Study the evaporation and spreading of the droplets in different diameters generated by coughing under different temperatures, humidity and breathing mean through the calculation with physical model and the droplet evaporation experiment.	When RH=0%, the horizontal influencing distance of 20μm droplets is greater than 4m, the horizontal influencing distance of 60μm droplets is about 2m, and the horizontal influencing distance of 100μm droplets is 1m. At the horizontal distance of 0.8m, the vertical scope of respiratory influence is about 0.3m, the vertical scope at the horizontal distance of 1.2m is about 0.4m, and the vertical scope at the horizontal distance of 1.6m is about 0.5m.
Zhang et al. 2019	Study the influence of different ventilation systems on the indoor spatial distribution of the droplets generated by coughing and breathing through LES CFD model coupling with the Lagrangian method and human body Simulation.	When the airflow velocity of breath exhalation is up to maximum, the scope of influence of the respiratory airflow is 0.12–0.14m, and the scope of influence of the airflow by coughing is 0.22–0.24m.
Xu et al. 2020	Study the influence of personalized ventilation means on the dilution of the concentration of the droplets exhaled by the person through the human body model simulation and the calculation with dose-response model, and evaluate the effect of the personalized ventilation in preventing the airborne transmission of infectious diseases in a short distance.	In the experiment, the distance between persons is set as 0.86m, and it is believed that the critical face-to-face condition with a relative distance <1m will be likely to transmit the infectious droplets through air in short distance.
Shafaghi et al. 2020	Study the distribution and spreading of the droplets generated by human breathing, coughing, and sneezing through CFD simulation based on the finite volume method and the calculation with numerical models, and give the safe horizontal distance for indoor population regarding the prevention of COVID-19.	The horizontal influencing distance of the droplets breathed by human body is less than 1m, the horizontal influencing distance of the droplets generated by sneezing is about 3m, and the horizontal influencing distance of the droplets generated by coughing is 6–7m. The vertical influencing distance of the droplets generated by sneezing is about 0.3m at the horizontal distance of 1m, and about 0.6m at 2m.

building as the roughness element. According to the urban morphology model Grimmond and Oke (1999) raised, RL is estimated with parameters such as building density and building height. SVF is estimated according to the geometric arrangement presented by Oke (1987) with the high-resolution digital building elevation model (Zhang et al. 2015). The local wind speed can be calculated with RL in the logarithmic law formula for urban background wind speed profile (Bañuelos-Ruedas et al. 2010; Mei et al. 2018). The related procedures are shown in Figure 3.

In this paper, according to the literature (Liu et al. 2019), the local wind speed within the grid is derived by aerodynamic roughness, and the accuracy is verified by the CFD method. 1 km^2 area of the study area is selected, and the wind speed simulation results of CFD software Phonics are compared with the calculation results of this paper. It can be seen from Figure 4 that the two have a good fit, which verifies the accuracy of the average wind speed calculation within the grid of this paper.

2.3 Module 3: calculation of the average number of contacts in a grid cell

In this paper, the initial value of the number of infected persons in the grid cell is set to 1, the immediate number of persons in the grid is N, and the average number of contacts I of infected persons in unit time is taken as the number of potential infected persons. The definition of the average number of contacts I: the average number of other people encountered by each infected person in a unit time. where the calculation about I is referred to the formula for calculating the average free range and average collision frequency of molecules. We obtain the average collision frequency of molecules in the two-dimensional case as follows (the average number of collisions per molecule with other molecules per unit time):

$$\bar{Z} = \sqrt{2} n d \bar{v} \tag{11}$$

where n is the total number of people in the 500 m grid, d is

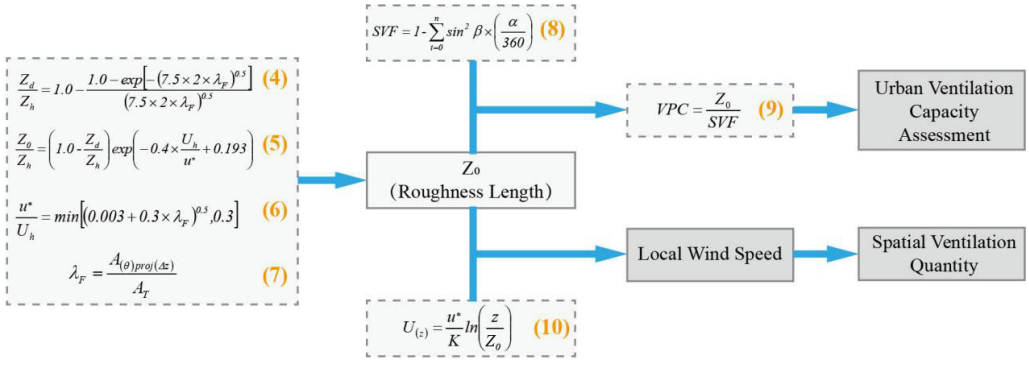

Fig. 3 Related formulas for urban ventilation environment assessment model

Notes: Roughness length: refers to the resistance incurred by surface roughness elements upon the airflow in the air. The wind speed on the wind speed profile is the height at the time of zero. **Sky view factor (SVF):** indicates the enclosing degree of urban space. The value ranges from 0 to 1. A value closer to 1 indicates a lower sky coverage rate. **Ventilation potential coefficient (VPC):** manifests the urban spatial ventilation capacity. The smaller the value, the higher the potential ventilation capacity could be. **Local wind speed:** urban environment factors affect local wind speed through influencing local roughness length. The results of local wind speed change with the height may be simulated with the Prandtl logarithmic law formula. **Equations (4)–(7):** Z_d is the displacement height on the zero plane (m), Z_0 is the roughness length (m), Z_h is the roughness element height (m), Z_d/Z_h is the zero-plane normalized displacement height, Z_0/Z_h is the normalized roughness length, U_h is the wind speed, u^* is the frictional speed, λ_F is the frontal area density of the urban buildings on the unit surface area, $A_{(\theta)proj(\Delta z)}$ represents the projected area on the frontal side of the building at certain height increments (Δz) and certain wind direction (θ); A_T indicates the standard unit grid under the bottom of the building (Wong 2010). **Equation (8):** α is the azimuth angle, β is the maximum building height angle in the sector of the corresponding azimuth angle within the study radius. $n=360/\alpha$, where the azimuth angle shall not be smaller than 36, that is, α shall be no more than 10°, and the value of radius (R) shall not be smaller than 20 (Wang et al. 2018). **Equation (9):** VPC is the ventilation potential coefficient (m), Z_0 is the aerodynamic roughness length, SVF is the sky view factor. **Equation (10):** $U_{(z)}$ is the average wind speed at the height z above the ground. In this paper, z is taken as the pedestrian walking height of 1.5 m, u^* is frictional speed, K is the Karman constant, which is generally approximately 0.4, and Z_0 is the aerodynamic roughness length.

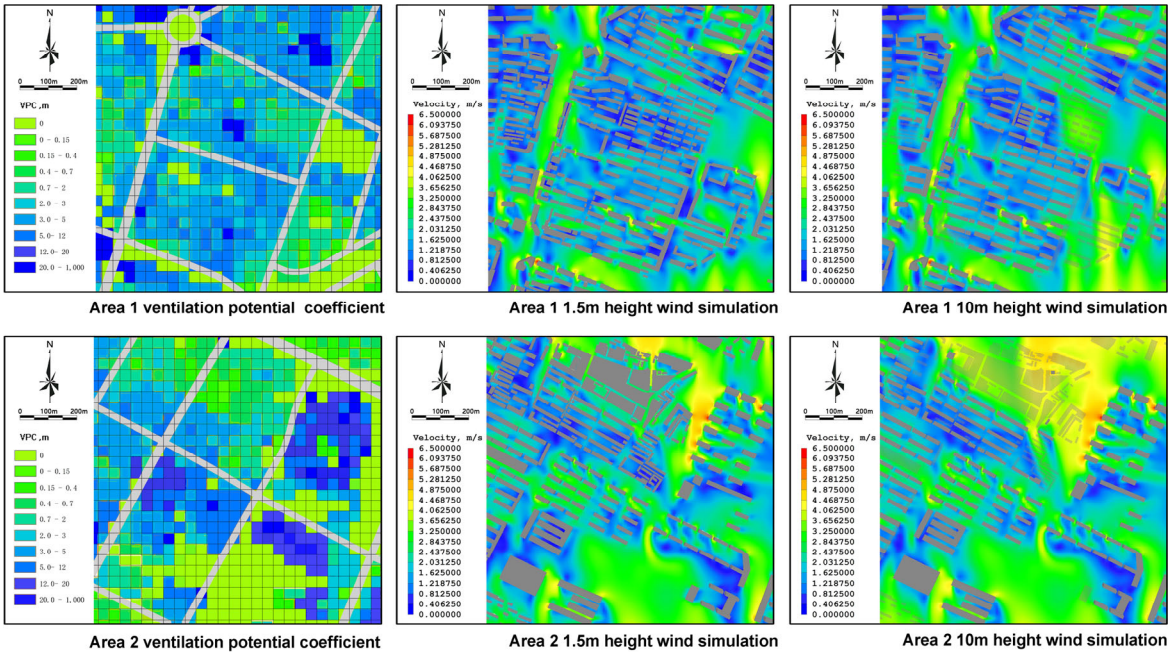

Fig. 4 Urban wind environment data validation analysis

the distance between two people, taken as 1 m, $\overline{v}$ is the average speed of movement of people, taken as 1–2 m/s.

Considering the influence of road network density on pedestrian flow, the road network density coefficient K is extracted from remote sensing data (Gong and Mo 2021), and the average number of contacts I is obtained by analogy as follows:

$$I = \sqrt{2}nd\overline{v}K \tag{12}$$

2.4 Module 4: Evaluation on respiratory infection intensity of the population on different types of the land

There is a significant time-space difference for the distribution

quantity of the population on different types of land in the city. To reflect the potential respiratory infection intensity of the people on different types of the urban area and thus to raise the control strategy for the various urban spaces. Our research has used the following evaluation model to obtain the respiratory infection risk intensity of the population on different types of the metropolitan area according to the calculation results of the infection probability in the abovementioned grid cell and combination with the spatial distribution data of the urban population:

$$E_L = \frac{\sum_{i=1}^{n}(P_i \times N_i)}{A_L} \tag{13}$$

where, E_L is the respiratory infection risk intensity of the population in the parcels of the city (persons/hm^2), P_i is the respiratory infection probability in grid i, N_i is the number of population in the grid i, n is the number of grids in the parcel, A_L is the parcel area, and L represents different parcels in the city.

3 Study area and methodology

3.1 Study area

This paper takes Shenyang city, Liaoning Province, China as the research object, which is a hub city in northeast China with dense and high mobility of population and more obvious characteristics of urban environment in severe cold areas. In this paper, an area of 45484.7 hm^2 within the 4th Ring Road of Shenyang was selected as the experimental area (Figure 5). In addition, we extracted a new round of Covid-19 epidemic data in the area between March and May 2022, and compared them with the simulated data to verify the validity of the experimental evaluation results in this paper.

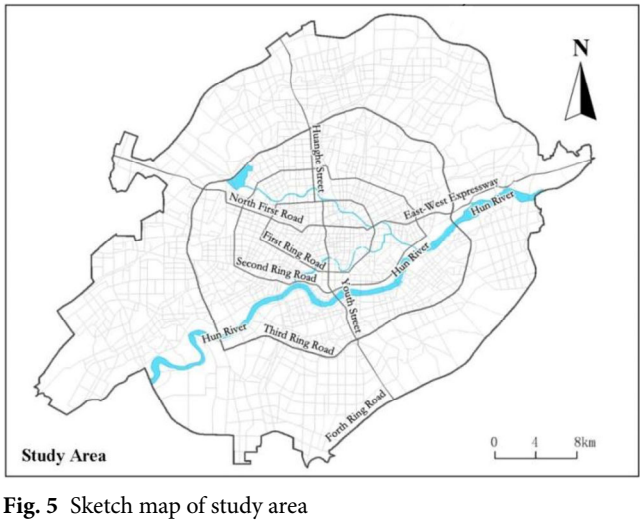

Fig. 5 Sketch map of study area

3.2 Data source and processing

It is based on urban satellite remote sensing images, urban 3D spatial information, meteorological data, and population flow monitoring data. Urban morphology data include Landsat8-OLI with 30 m resolution in 2020 and Quickbird image data with 2 m resolution in 2020 within the 4th Ring Road of Shenyang, Shenyang city General Urban Planning (2011–2020) and 1:2000 mapping of the current situation of buildings and roads in Shenyang. The meteorological data include Shenyang city 2016–2019 meteorological data. The population distribution and flow monitoring data include the results of the sixth national census to get the data of the resident population within the Third Ring Road of Shenyang, the data of cell phone base stations for multiple periods on April 23, 2020, and the extraction of spatial heat distribution data of outdoor population.

3.3 Setting of risk variables based on multiple scenarios

This study has made a comparative analysis on the distribution characteristics of infection risks under different variables by considering multiple scenarios with the gridded population, the distance between persons, exposure time, and average background wind speed (Table 2). And we use these multiple scenarios to discuss the influence of different urban environmental elements on the distribution of respiratory infection risks. According to the calculation results of infection probability in multiple scenarios, SPSS analyzes the correlations between the variables and the infection probability and dangers. Concerning monitoring the population flow data, the data collection was conducted during days off and working days. The spatial distribution data for the outdoor population in Shenyang city during multiple periods from March 15 to May 25, 2020, was chosen as the basis for the value assignment of the potentially infected population coefficient within the grid.

4 Results and analysis

4.1 Analysis on the spatial distribution change of the population

Figure 6 shows the statistical results for the thermal capacity distribution of the population study during a typical working day (April 23). In this part, we used the method in which the number of points for the outdoor population

Table 2 Setting of the variables in multiple scenarios for evaluation of respiratory infection risks in Shenyang city

Variable setting	Description	Variable values in various scenarios								
		Initial	Scenario 1	Scenario 2	Scenario 3	Scenario 4	Scenario 5	Scenario 6	Scenario 7	Scenario 8
Coefficient of potential infected persons, I (persons)	Mean value of the outdoor population in the time periods of typical working days in Shenyang city for the grids, whose logarithmic function is taken for the weight estimation	$w\times N$	$\boldsymbol{w\times 0.5N}$	$\boldsymbol{w\times 1.5N}$	$w\times N$	$w\times N$	$w\times N$	$w\times N$	$w\times N$	$w\times N$
Exposure time, t (min)	Analyze the relations between the infection probability and the retention time of the people in public space based on the different retention time of the people in public space	20	20	20	**15**	**25**	20	20	20	20
Distance between persons, D (m)	Explore the influence of distance between persons on the respiratory infection risks based on the different distances between persons	1	1	1	1	1	**1.5**	**2**	1	1
Average background wind speed, $\overline{U}$ (m/s)	Refer to average annual wind speed and the wind scale with high frequency in the second quarter in Shenyang city	3	3	3	3	3	3	3	**2**	**4**

Note: w is the weight coefficient which is multiplied in estimating the number of infected persons.

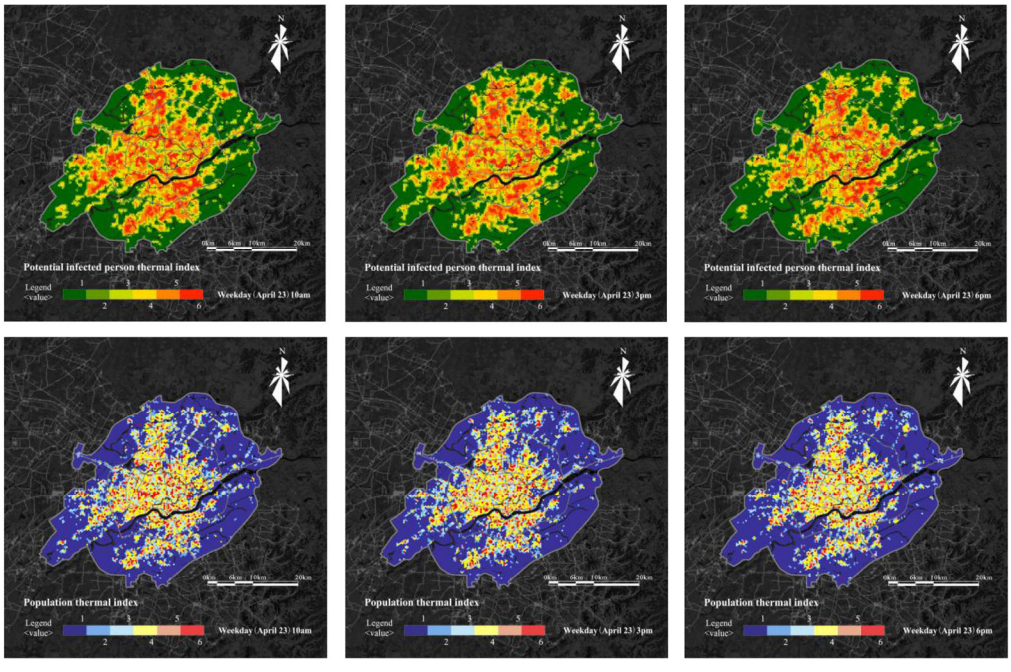

Fig. 6 Spatial distribution of the outdoor population in different time periods on a typical working day

is extracted for kernel density analysis (Wu and Ye 2016; Lan et al. 2018). The case can be classified into six levels of thermal capacity, from high to low, as determined by the cluster analysis. High thermal areas and sub-thermal areas corresponding to the red and orange zones can represent the highly populated zone of urban people. And the result can show the main area for the activities people partake in in public spaces (Li et al. 2019).

The trend of the heated area with time shows that the red high heat area on weekdays is higher at 10:00 p.m., relatively decreases at 3:00 p.m., and is lower at 6:00 p.m. The spatial distribution of the high-heat and sub heat areas shows that the dense human activity areas mainly exist in the commercial and transportation hub areas within the First Ring Road.

There is a clear decreasing trend of population density from the First Ring Road to the Second and Third Ring Roads.

4.2 Analysis on the ventilation capacity in urban public spaces

Figure 7 shows the assessment results of ventilation capacity on the ground surface within the Fourth Ring Road of Shenyang city. The basic morphology parameters of building height (BH), building density (BD), and frontal area density (FAD) are extracted, and calculation is performed with Eqs. (4)–(7) to obtain the spatial distribution of aerodynamic roughness length (RL) in Figure 3. It may be seen from Figures 7(a)–(d) that the roughness length has a high degree of fitting with the change of building height distribution, and the old downtown area within the First Ring Road is basically covered by a high-value zone (RL > 2). BH and RL are at the highest level on the south of Hun River outside the Second Ring Road. High-rise buildings are densely distributed, creating a large ventilation barrier region. BD and FAD have a similar distribution. Aside from the high-rise buildings within the First Ring Road, there is still a sizeable high-density zone on the urban-suburban residential land and industrial land at the edge of Third Ring Road.

Figure 7(e) shows the spatial distribution of sky view factor (SVF), which gradually increases from the city center to the surrounding areas, and reaches the minimum value in the area on the south of Hun River, where SVF remains in the interval of 0–0.42 because, in this region, the building density is not high. Still, the building height reaches the maximum level within the Third Ring Road, and the sky is highly sheltered due to building height. Figure 7(f) shows the potential ventilation coefficient, where there is a sizeable high-value area with poor ventilation (VPC > 3.8 m), covering nearly half of the area within the Third Ring Road, with the radial extension from the old downtown area within the First Ring Road. At the same time, there is the poorest ventilation in the area with large roughness and low sky view factor in the area on the south of Hun River. It can be seen from the above analysis that urban surface ventilation capacity is significantly affected by spatial morphology, and the local environment has a big difference in wind speed. In meteorological conditions with low urban background wind speed, the ventilation effect of some parcels will be less desirable, increasing respiratory infection risk probability.

4.3 Influence of multiple variables on respiratory infection risk in urban spaces

Our calculation was performed with Eqs. (1)–(13) to obtain the distribution of infection probability risk levels on a typical working day (Figure 8). After the cluster analysis, the risk areas were classified into high-risk area (3.5%–5%),

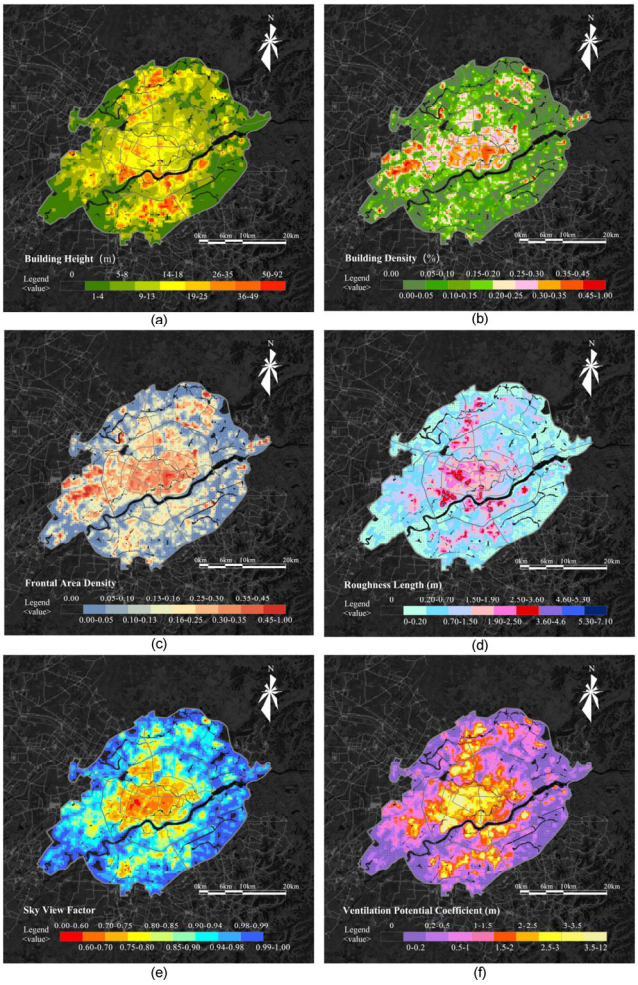

Fig. 7 Spatial distribution of main parameters for the surface ventilation capacity evaluation in the main downtown area of Shenyang city: (a) building height; (b) building density; (c) frontal area density; (d) roughness length; (e) sky view factor; (f) ventilation potential coefficient

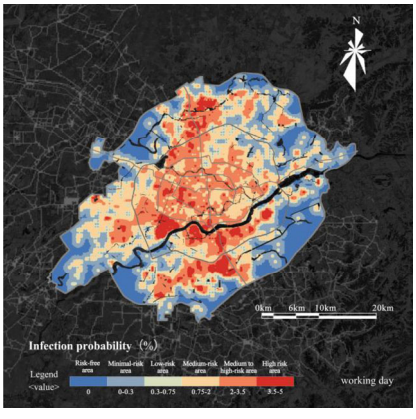

Fig. 8 Distribution of infection probability risk levels on a typical working day in the main downtown area of Shenyang city

medium to high-risk area (2%–3.5%), medium-risk area (0.75%–2%), low-risk area (0.3%–0.75%), minimal-risk area (0%–0.3%), and risk-free area (0%). Different from the distribution of outdoor population, the high infection probability area mainly concentrates on both sides of the north-south axis of the city (Youth Street) and the south of Hun River outside the Second Ring Road. Some other high-risk points are mostly distributed within the First Ring Road and sporadically distributed between the First Ring Road and the Second Ring Road and on the edge of the Second Ring road.

Considering changes in human body spacing, exposure time, number of potential infections, and background mean wind speed, the distribution of infection probability in urban public space obtained according to the multiple scenarios set in Section 3.3 is shown in Figure 9. The trend of changes in each risk area is consistent under different scenarios, but there are large differences in the area of risk levels. In order to further explore the degree of influence of each variable on the probability of infection, the correlation analysis of population number N, the exposure time t, the human body spacing D, the background mean wind speed $\overline{U}$ and the change of area of each risk area was conducted using SPSS. The results of the analysis are shown in Table 3, and all four variables and the area of each risk area passed the significance verification. Among them, population size and exposure time were positively correlated with the increase of infection probability, while human body spacing and background mean wind speed were negatively correlated with the increase of infection probability. The mean absolute values of the correlation coefficients of population size, exposure time, human body spacing, and background mean wind speed in each risk area were 0.618, 0.612, 0.632, and 0.752, respectively, which showed that the significance of the above four variables on the degree of infection risk was: background mean wind speed > human body spacing > number of potential infections > exposure time.

Four variables were selected to establish a one-dimensional linear equation with the change in the area of the high-risk area as shown in Figure 10, and the R^2 of N, t, D, and $\overline{U}$ with the area of the high-risk area were 0.900, 0.823, 0.407, and 0.540, respectively, indicating that two of the variables, number and exposure time, had the strongest degree of correlation on the results. Meanwhile, from the trend of point distribution in the figure, population number and exposure time have a significant positive linear relationship with the change of area of high-risk area, and their influence on the change of results continues to increase with the change of variables, while both variables, human body spacing and background wind speed, show limitations in the trend of point distribution on the results, i.e., the results tend to be stable and unchanged after the values of variables reach a specific value. Therefore, in the prevention and control of respiratory infectious disease, reasonable control of human density and reduction of exposure time in public space are the most effective measures to reduce the risk of infection. From the scatter diagram, it can be seen that

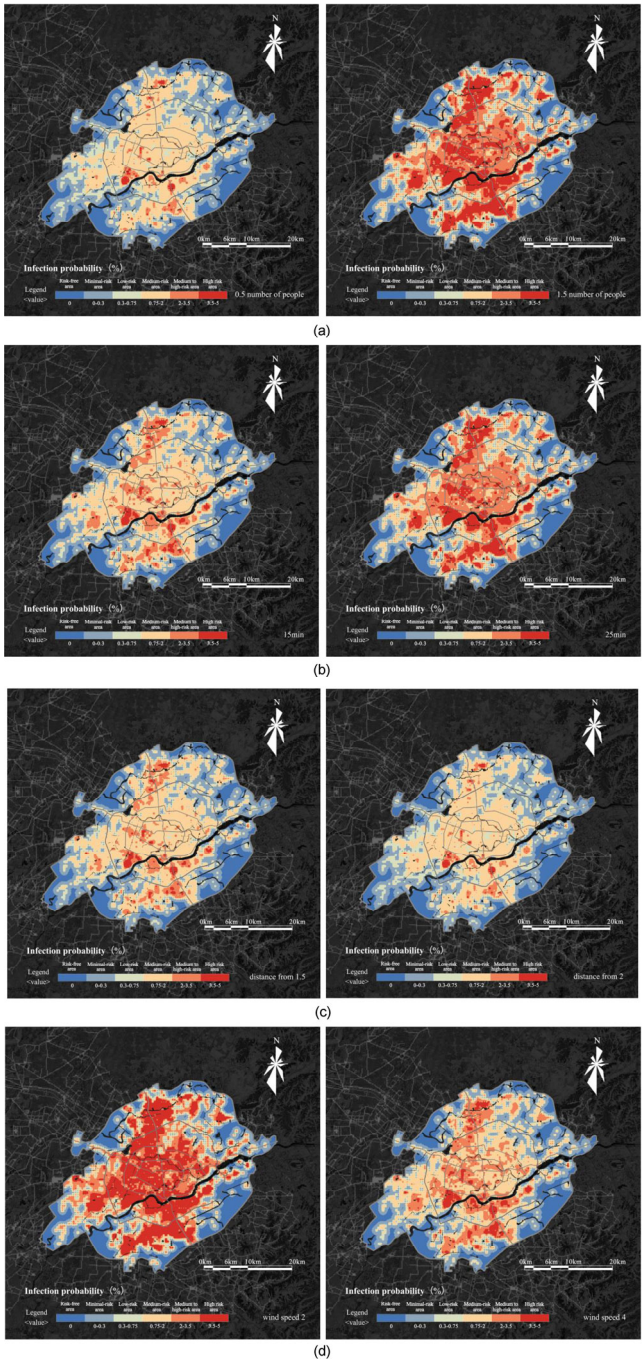

Fig. 9 Distribution of risk levels for infection probability on a typical working day with multi-variable settings in the main downtown area of Shenyang city: (a) 0.5 times and 1.5 times the number of population; (b) exposure time 15 min, 25 min; (c) distance between persons 1.5 m, 2 m; (d) average background wind speed 2 m/s, 4 m/s

Table 3 Correlation analysis of each group of variables with changes in regional infection risk

Different variables	High-risk area (3.5%–5%)	Medium to high-risk area (2%–3.5%)	Medium-risk area (0.75%–2%)	Low-risk area (0.3%–0.75%)	Minimal-risk area (0%–0.3%)	Risk-free area (0%)
Number of population N	0.948**	−0.472*	−0.726**	−0.521*	−0.421	—
Exposure time t	0.907**	−0.580**	−0.708**	−0.476*	−0.388	—
Distance between persons D	−0.638**	0.512*	0.682**	0.808**	0.520*	—
Average background wind speed $\bar{U}$	−0.735**	−0.801**	0.448*	0.904**	0.871**	—

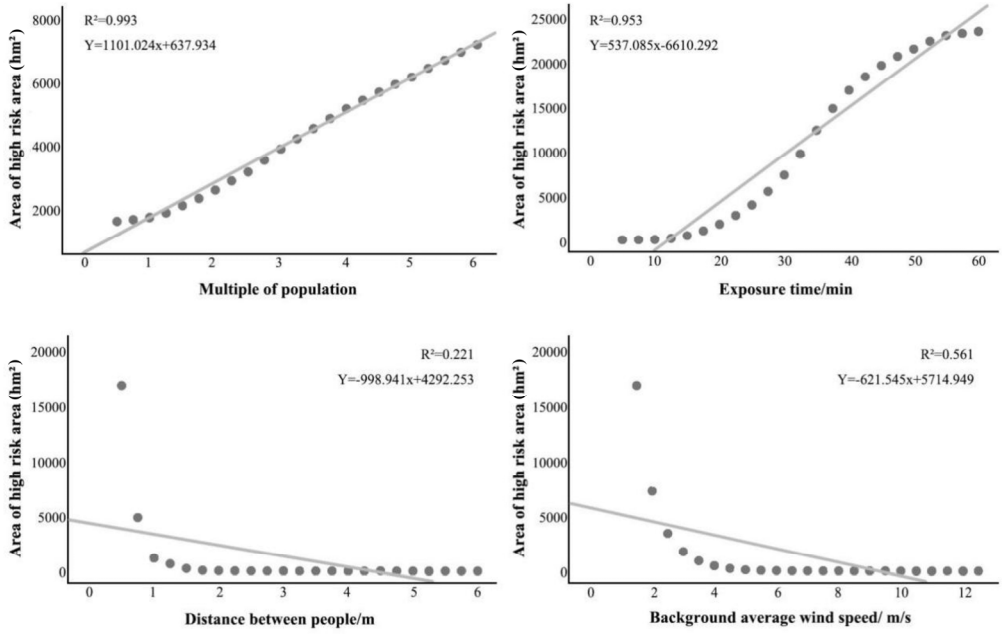

Fig. 10 Scatter plot and linear equation for different variables and the change of the area in the zone with high infection probability in Shenyang city

the area of high risk area increases significantly when the human body spacing is less than 1 m, so reasonable control of safety distance in public activities is also a scientific and effective control measure.

From the data analysis results, the background wind speed has a moderate correlation with the change of the risk area. From the analysis on the correlation between the urban morphology parameters (building height (BH), building density (BD), roughness length (RL), sky view factor (SVF) and the change of risk levels, it can be known that the performance of the correlation between four parameters and the change of risk levels is BH (0.837) > RL (0.721) > SVF (−0.286) > BD (0.018). Figure 11 is the box plot for the distribution of urban morphology parameters in the risk levels, and after the elimination of the influence of abnormal values, it can be clearly seen that the numerical distribution interval values of BH and RL increase significantly with the rise of the risk level, and have relatively low data fluctuation; the interval values of BH and SVF have weak law of distribution in the different risk areas, and the maximum and minimum values of the interval and the quartile are far from the median value and have strong data dispersion. Therefore, improving the local ventilation environment in the city by optimizing the urban spatial morphology also plays an important role in reducing infection risk probability, while adjusting building height and roughness length can achieve a better optimization effect.

We also conducted a correlation analysis between urban green space, water body area, and POI. We can find that the feedback of POI (population activity points of interest) on the results are self-explanatory, and its values are all higher in high-risk areas, while they tend to be lower in low-risk areas. We found that the median values of green areas and water bodies in high-risk areas were lower. The median values of green areas and water bodies in low-risk areas were higher, indicating that changes in green areas and water bodies seem to impact the risk of virus infection. However, there was no significant change in the overall values. This also indicates that the changes in green areas and water bodies do not directly affect the risk of virus infection. As for the trend in the figure below, we believe

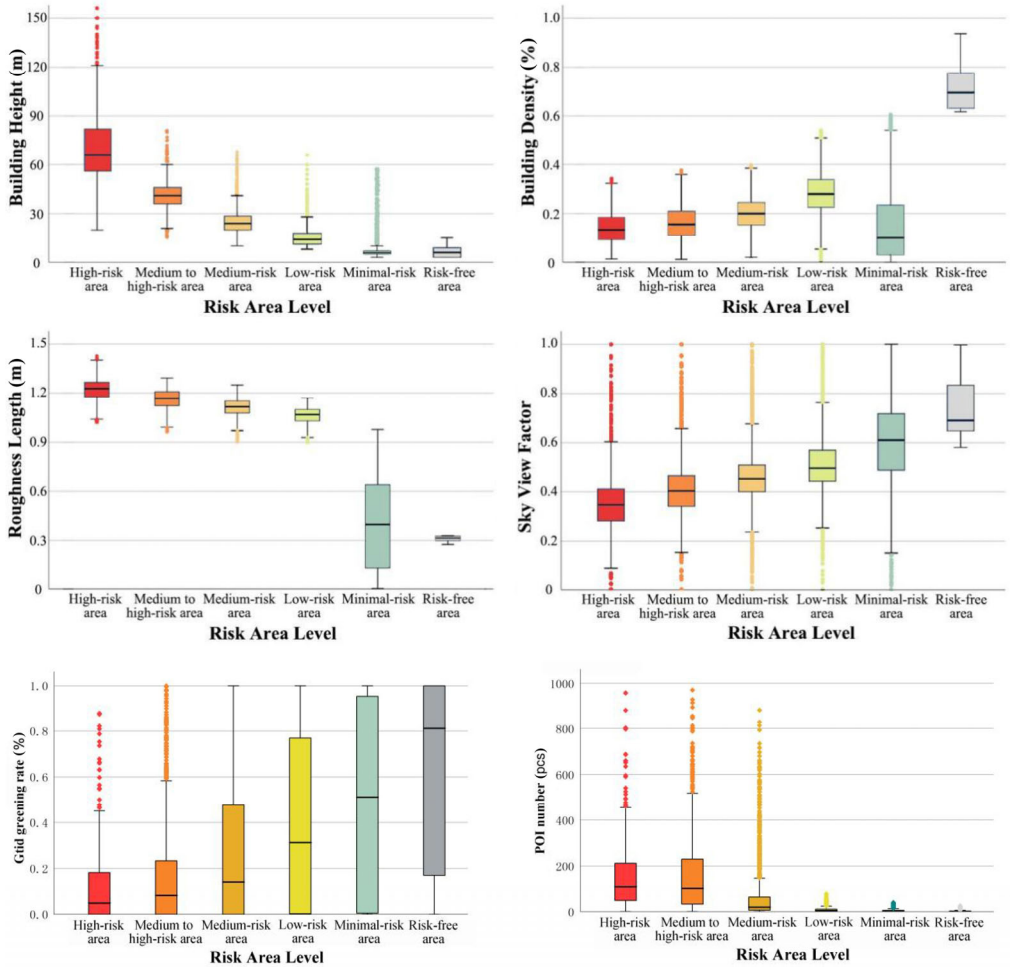

Fig. 11 Box plot for urban morphology parameters in the risk areas

that the changes in green space and water bodies indirectly affect human behavior patterns, which weakly affects the risk of virus infection. The above results are also more consistent with our initial considerations when designing the model.

4.4 Validation of the results of infection risk zone classification

Of the 274 actual cases in the study area, the number of cases distributed within the risk level was 271, accounting for 98.91%. Among them, 58 cases were in the high-risk zone of infection probability, accounting for 21.17%; 99 cases were in the medium-high risk zone, accounting for 36.13%; 59 cases were in the medium-risk zone, accounting for 21.53%; 21 cases were in the low-risk zone, accounting for 7.67%; 34 cases were in the micro-risk zone, accounting for 12.41%; and 3 cases were in the no-risk zone, accounting for 1.09% (Figure 12). The overlap between the medium-risk or higher area and the actual cases was 78.55%, indicating that the risk partition of infection probability is reasonable, which can effectively predict the high-risk incidence area and take preventive measures in advance.

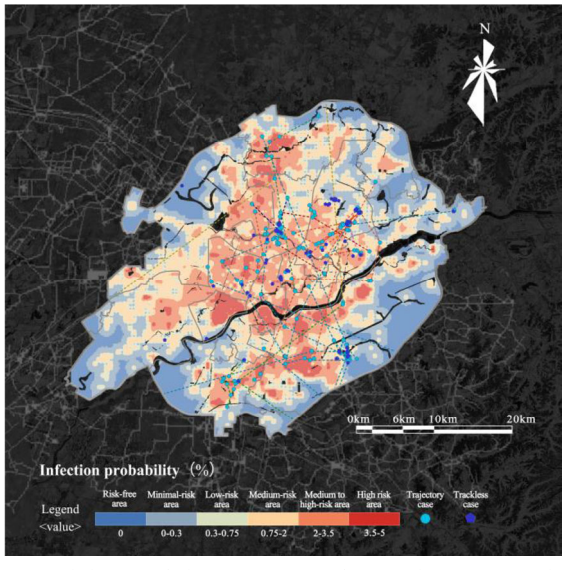

Fig. 12 Validation of Shenyang case infection data compared with simulation results

5 Discussion

5.1 Influence of urban morphology on the risk distribution of outbreak infection

The above evaluation results show that urban morphological parameters are important factors affecting the risk of respiratory infection in public spaces. From the viewpoint of building height, the average level inside the Second Ring Road is higher than that outside the Second Ring Road, while the average level along the south side of Hun River is the highest in the city. The building density is not related to the urban radial structure, and high-density spaces exist in both old and new urban areas. The local area between the Second and Third Ring Roads is even higher than the old urban area. The population distribution pattern shows a decreasing trend from the central area of the city to the outer ring area, and there is apparent spatial heterogeneity of various elements. The spatial distribution characteristics of the probability of infection risk are a significantly better fit with urban morphological parameters than with spatial population distribution, and "building high-density space" tends to be more consistent with the characterization of a respiratory infection risk than "population high-density space". In addition, exposure time and body spacing have a more significant influence on the risk of infection. These two parameters depend on the activity pattern of the population in public spaces. Urban spatial morphology and environment also indirectly influence the activity pattern of the population. Thus, the spatial distribution of infection risk is closely related to urban morphology and human activity patterns. Urban morphology potentially influences the degree of infection risk of an epidemic through the influence of local microclimate and the guidance of population activity patterns.

5.2 Population respiratory infection risk intensity by site type

Calculations were made according to the planned land use situation in Shenyang city to obtain the respiratory infection risk intensity distribution map of the population in different parcels (in Figure 13), which disclosed the correlations between various types of land and respiratory infection risk. From the analysis on the area proportion of multiple types of land in Figure 14(a), it can be seen that the higher proportion of residential land in the central downtown area accounts for a large proportion of all risk levels. In addition, the core business districts of Shenyang city are concentrated within the First Ring Road, thus seeing dense population activities. Therefore, in a high-risk area, land used for the facilities of commercial and business industries accounts for a very high percentage. The potential infection risk intensity was further analyzed after the normalization of various land indexes. As seen from Figure 14(b), residential land is the category with the highest intensity of urban infection risk, followed by commercial land and public service land, with the three categories accounting for more than 80% of the land use. Residential land as the most concentrated area of urban population activities, the general high density of old residential areas and the obvious growth of residential height in new urban areas will lead to poor local ventilation capacity and increase the risk of respiratory infection. So this type of land also occupies a high proportion in high-risk and higher-risk areas. The commercial space itself is a frequent area of urban population activities, and the core commercial areas of Shenyang are closely linked to the city's major transportation hubs. In the land for residential use, which represents the area with the highest concentration of activities for the urban population, the old residential zones generally have high density, and the height of residential buildings in new urban areas increases significantly. Both will result in poor local ventilation and increasing the risk of respiratory infection. Under these circumstances, such land types account for a high proportion of the high-risk and medium to high-risk areas. The above evaluation results align with the statistical distribution of epidemic cases in the cities. So, land for commercial and business facilities and land for residential should be the key zones for epidemic prevention in cities. In addition, it can be seen from the

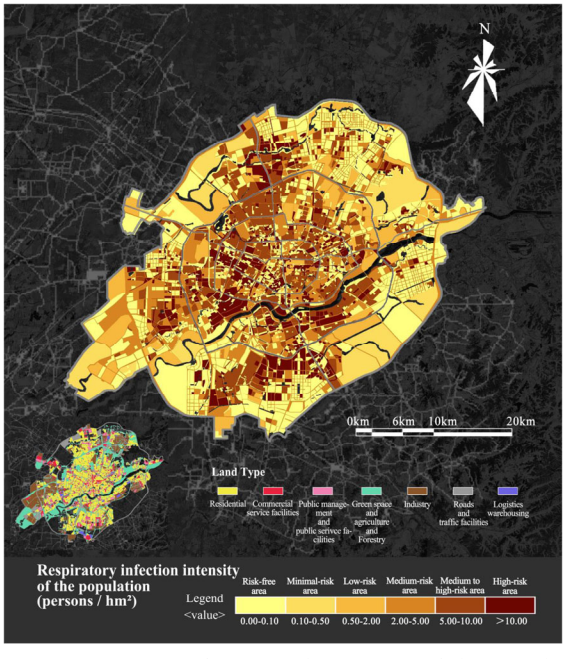

Fig. 13 Respiratory infection risk intensity of the population on different types of land in the main downtown area of Shenyang city

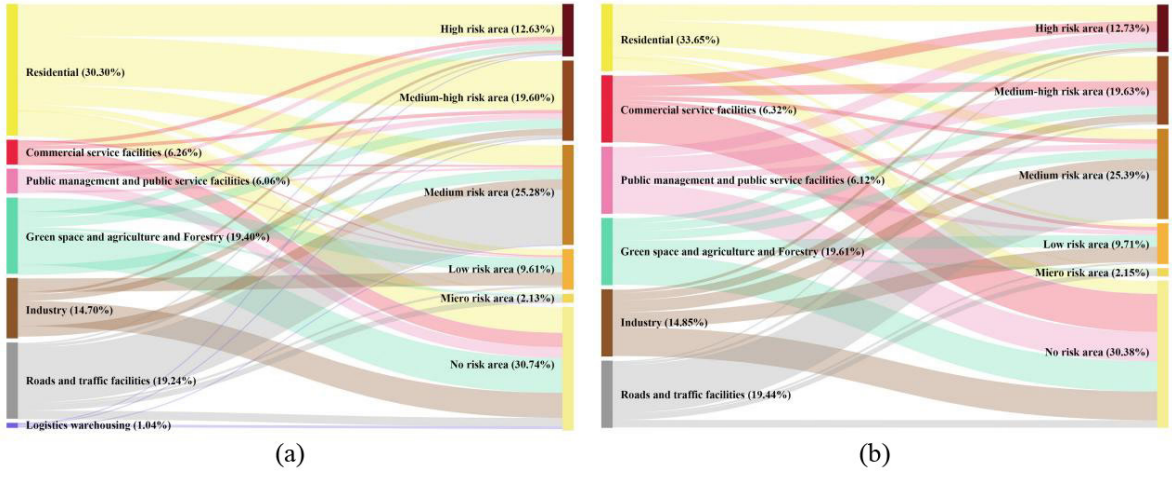

Fig. 14 Proportion of different types of land in risk areas in the main downtown area of Shenyang city: (a) proportion of different types of land in the risk areas; (b) the proportion of the main types of land in the risk areas after normalization

analysis that administration and public services land, such as administrative offices, medical, and educational use, is also a critical control area in epidemic prevention and control due to regular human activities. At the same time, industrial-use land with low spatial density and low building height have low infection risk levels.

5.3 Normalized strategy for epidemic prevention in public spaces in cities

(1) Urban spatial morphology should be optimized and ecological elements adequately allocated. The influence of urban spatial morphology parameters on the respiratory infection risks shows that ventilation barrier areas are easily created in high-density urban spaces, which is unfavorable for the dissipation of air pollutants. Thus the local environment is poor in coping with outbreaks. Therefore, in planning and urban design, more importance should be attached to the impact of spatial morphology on the local microclimate, water cycle, and biodiversity, thus organizing the spatial morphology in a manner favorable for optimizing the ecological process. And reasonable allocation of spatial elements, such as green spaces and open spaces, and the construction of ventilation galleries not only meet the aesthetic requirements of urban design but also benefit citizens in developing positive emotions, and also serve as an essential guarantee for the healthy development of a city, improving urban inclusion and the ability to deal with emergencies in case of epidemics (Yang et al. 2020).

(2) From the analytical results of the infection risk intensity on various types of land in the city, it can be seen that residential community, commercial, and office spaces have relatively high population density and comprehensive urban development intensity as well as generally high infection risk levels. This is consistent with the statistical results of the infection fields for diseases worldwide. Therefore, strengthening the real-time monitoring of high-risk spaces and the management of mass gatherings, limiting population density, and controlling the exposure intensity of the population are effective measures to reduce the propagation risk of epidemics. Taking communities, streets, and villages as the primary managing and controlling units and starting from the community for accurate implementation of prevention and control measures is the current key for normalized epidemic prevention in China (Duan et al. 2020; Liu 2020) and may also serve as a reference for the cities of other countries in the world.

(3) The scale of the control unit is explored in comparison with the distribution of medical resources. Currently, in China's cities, during the period of concentrated outbreaks, most of the closed control measures are based on the spatial unit of residential areas, which may have adverse effects on the psychological aspects of residents due to the limited range of activities during the closed period. Under the premise of improving community functions and management capabilities, appropriate expansion of the control unit can solve some of the citizens' work, commercial, and sports activities in the community, significantly alleviating the anxiety caused by the closure. Figure 15 is the division of control units based on the 15-minute living circle in Shenyang. The unit's color represents each control unit's comprehensive infection risk index, and each point is the distribution of medical resources at different levels. In the units with a high comprehensive infection risk index, only the central city is more affluent in medical

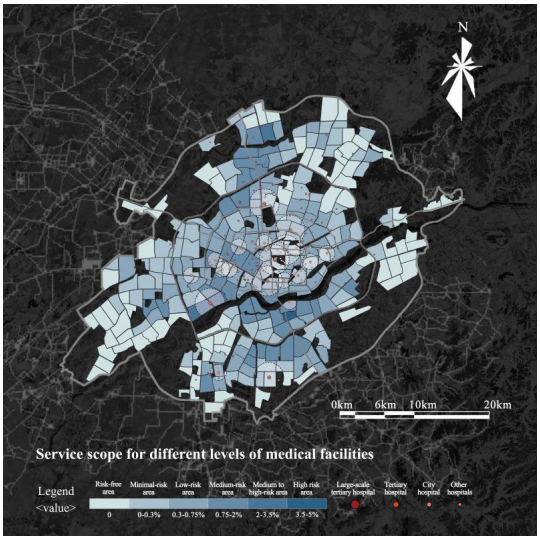

Fig. 15 Service scope for different levels of medical facilities

resources. In contrast, in the units with more high-risk areas in the north and south, the degree of matching the level and quantity of medical resources is lower.

(4) Scientific guidance for urban activities and behavioral modes is essential. The research results in the multi-scenario setting have shown that reasonable control of human physical distance and exposure time can reduce regional infection probability. In this case, guiding individual activity morphology and behavioral characteristics is necessary to curb the spread of the epidemic. Officials can develop the safety threshold of the related parameters for citizens in different places when risk levels are formed in urban areas (Mehta 2020; Sun and Zhai 2020), put forward necessary prevention guidelines, monitor people's health and safety conditions, and provide safety measures for the communication and interaction of the susceptible population in public spaces, such as the elderly, children and pregnant women.

5.4 Disadvantages and future development

In this study, since there is no more traditional calculation method for estimating outdoor public space ventilation, this paper refers to the existing results in the literature. It proposes a method for estimating the instantaneous airflow within the respiratory influence of sick patients under ideal conditions to estimate the probability of respiratory infection in a grid cell. Secondly, in estimating the urban local ventilation environment, we only considered the influence of building space morphology on ventilation, and elements such as green space and water bodies on air quality were not included in the model. In future studies, these need to be discussed in-depth to improve the accuracy of this evaluation model.

6 Conclusion

The novel coronavirus epidemic has made us re-examine the impact of the urban spatial environment on public health, and it is urgent to develop an urban planning system that can guarantee public health and health safety in cities. This paper aims to construct an urban-scale risk assessment method for respiratory infections in public spaces and use spatial GIS to form a visual map to provide dynamic risk warning for high-risk areas in cities. So that city managers can formulate specific risk intervention countermeasures in response to the spatial differentiation characteristics of risk elements, and control the safety of public activities in cities in a timely manner during the normalization phase of the epidemic, and shift the responsibility to the new coronavirus epidemic from a "reactive emergency mode" to a "reactive emergency mode". This will change the response to the Covid-19 epidemic from a "reactive emergency mode" to a "proactive prevention and control mode".

On the other hand, creating resilient cities that can resist risks and recover quickly has become a consensus in urban planning and design after the outbreak. What kind of urban structure and spatial form is more conducive to constructing resilient cities? How do optimize the configuration of public open space and ecological infrastructure to create a healthy local climate environment? These questions are still at the preliminary stage of exploration. And establishing a data platform to reveal the coupling relationship between urban environment and population can provide sufficient scientific support to analyze and explain these fundamental questions. This is also the exploratory research of this paper for the construction of urban public safety and resilient cities through the precise evaluation of the risk of Covid-19 infection in urban space.

Acknowledgements

This project was financially supported by the General Program of National Natural Science Foundation of China (No. 51978421). The authors express their sincere gratitude to all members of the research team for their invaluable contributions.

Declaration of competing interest

The authors have no competing interests to declare that are relevant to the content of this article.

References

Azevedo L, Pereira MJ, Ribeiro MC, et al. (2020). Geostatistical COVID-19 infection risk maps for Portugal. *International Journal of Health Geographics*, 19: 25.

Bañuelos-Ruedas F, Angeles-Camacho C, Rios-Marcuello S (2010). Analysis and validation of the methodology used in the extrapolation of wind speed data at different heights. *Renewable and Sustainable Energy Reviews*, 14: 2383–2391.

Borak JS, Jasinski MF, Crago RD (2005). Time series vegetation aerodynamic roughness fields estimated from modis observations. *Agricultural and Forest Meteorology*, 135: 252–268.

Buonanno G, Stabile L, Morawska L (2020). Estimation of airborne viral emission: Quanta emission rate of SARS-CoV-2 for infection risk assessment. *Environment International*, 141: 105794.

Chen SC, Liao CM (2008). Modelling control measures to reduce the impact of pandemic influenza among schoolchildren. *Epidemiology and Infection*, 136: 1035–1045.

Chen Y, Yang K, Zhou D, et al. (2010). Improving the Noah land surface model in arid regions with an appropriate parameterization of the thermal roughness length. *Journal of Hydrometeorology*, 11: 995–1006.

Dai H, Zhao B (2020). Association of the infection probability of COVID-19 with ventilation rates in confined spaces. *Building Simulation*, 13: 1321–1327.

Dlamini WM, Dlamini SN, Mabaso SD, et al. (2020). Spatial risk assessment of an emerging pandemic under data scarcity: A case of COVID-19 in Eswatini. *Applied Geography*, 125: 102358.

Duan J, Yang B, Zhou L, et al. (2020). Planning improves city's immunity: A written conversation on COVID-19 breakout. *City Planning Review*, 44(02): 115–136. (in Chinese)

Furuya H (2007). Risk of transmission of airborne infection during train commute based on mathematical model. *Environmental Health and Preventive Medicine*, 12: 78–83.

Gong S, Mo H (2021). Geographic analysis of the COVID-19 epidemic in Hunan Province in 2020. *Tropical Geography*, 41(04): 708–722. (in Chinese)

Gralton J, Tovey E, McLaws ML, et al. (2011). The role of particle size in aerosolised pathogen transmission: a review. *Journal of Infection*, 62: 1–13.

Grimmond CSB (1998). Aerodynamic roughness of urban areas derived from wind observations. *Boundary-Layer Meteorology*, 89: 1–24.

Grimmond CSB, Oke TR (1999). Aerodynamic properties of urban areas derived from analysis of surface form. *Journal of Applied Meteorology*, 38: 1262–1292.

Gualtieri G, Secci S (2011). Wind shear coefficients, roughness length and energy yield over coastal locations in Southern Italy. *Renewable Energy*, 36: 1081–1094.

Jacobs J (1964). The Death and Life of Great American Cities. Harmondsworth, UK: Penguin Books.

Jiang P, Fu X, Fan YV, et al. (2021). Spatial-temporal potential exposure risk analytics and urban sustainability impacts related to COVID-19 mitigation: A perspective from car mobility behaviour. *Journal of Cleaner Production*, 279: 123673.

Kamel Boulos MN, Geraghty EM (2020). Geographical tracking and mapping of coronavirus disease COVID-19/severe acute respiratory syndrome coronavirus 2 (SARS-CoV-2) epidemic and associated events around the world: How 21st century GIS technologies are supporting the global fight against outbreaks and epidemics. *International Journal of Health Geographics*, 19: 8.

Kang JY, Michels A, Lyu F, et al. (2020). Rapidly measuring spatial accessibility of COVID-19 healthcare resources: a case study of Illinois, USA. *International Journal of Health Geographics*, 19: 36.

Lan T, Yu M, Xu Z, et al. (2018). Temporal and spatial variation characteristics of catering facilities based on POI data: A case study within 5th ring road in Beijing. *Procedia Computer Science*, 131: 1260–1268.

Li J, Li J, Yuan Y, et al. (2019). Spatiotemporal distribution characteristics and mechanism analysis of urban population density: A case of Xi'an, Shaanxi, China. *Cities*, 86: 62–70.

Li S, Chen Y, Shi T, et al. (2020). Risk assessment of respiratory exposure in urban public space for air epidemic prevention. *City Planning Review*, 44(08): 21–32. (in Chinese)

Liu L, Wei J, Li Y, et al. (2017). Evaporation and dispersion of respiratory droplets from coughing. *Indoor Air*, 27: 179–190.

Liu Y, Xu Y, Zhang F, et al. (2019). Research and application of urban surface ventilation potential: Cases of Beijing and Guangzhou. *Planners*, 35(10): 32–40. (in Chinese)

Liu J (2020). Community epidemic prevention planning and govemance system against COVID-19 epidemic. *Planners*, 36(6): 86–89. (in Chinese)

Mehta V (2020). The new proxemics: COVID-19, social distancing, and sociable space. *Journal of Urban Design*, 25: 669–674.

Mei F, Zhang N, Xi Y, et al. (2018). The aerodynamic roughness length over rough surfaces derived from whole wind velocity profiles with the log law and its spatial variations. *Journal of Desert Research*, 38(03): 445–454. (in Chinese)

Noakes CJ, Beggs CB, Sleigh PA, et al. (2006). Modelling the transmission of airborne infections in enclosed spaces. *Epidemiology and Infection*, 134: 1082–1091.

Noakes CJ, Sleigh PA (2008). Applying the Wells-Riley equation to the risk of airborne infection in hospital environments: The importance of stochastic and proximity effects. In: Proceedings of the 11th International Conference on Indoor Air Quality and Climate (Indoor Air 2008), Copenhagen, Denmark.

Oke TR (1987). Boundary Layer Climates. London: Routledge.

Peixoto PS, Marcondes D, Peixoto C, et al. (2020). Modeling future spread of infections via mobile geolocation data and population dynamics. An application to COVID-19 in Brazil. *PLoS One*, 15: e0235732.

Qian H, Li Y, Nielsen PV, et al. (2009). Spatial distribution of infection risk of SARS transmission in a hospital ward. *Building and Environment*, 44: 1651–1658.

Qian H, Zheng X, Zhang X (2012). Prediction of risk of airborne transmitted diseases. *Journal of Southeast University* (*Natural Science Edition*), 42(03): 468–472. (in Chinese)

Riley EC, Murphy G, Riley RL (1978). Airborne spread of measles in a suburban elementary school. *American Journal of Epidemiology*, 107: 421–432.

Shafaghi AH, Rokhsar Talabazar F, Koşar A, et al. (2020). On the effect of the respiratory droplet generation condition on COVID-19 transmission. *Fluids*, 5: 113.

Sun C, Zhai Z (2020). The efficacy of social distance and ventilation effectiveness in preventing COVID-19 transmission. *Sustainable Cities and Society*, 62: 102390.

Tibbalds F (1992). Making People-Friendly Towns: Improving the Public Environment in Towns and Cities. Harlow, UK: Longman.

Urrego J, Andrews JR, Yeckel CW, et al. (2015). The impact of ventilation and early diagnosis on tuberculosis transmission in Brazilian prisons. *The American Journal of Tropical Medicine and Hygiene*, 93: 739–746.

Villafruela JM, Olmedo I, Ruiz de Adana M, et al. (2013). CFD analysis of the human exhalation flow using different boundary conditions and ventilation strategies. *Building and Environment*, 62: 191–200.

Wang Z, Cheng C, Yang Y, et al. (2018). Research on urban ventilation channel planning strategy which based on multivariate date analysis: Take Beijing sub center as an example. *Urban Development Studies*, 25(01): 87–96. (in Chinese)

Wang J, Li G, Wang J, et al. (2020). Spatiotemporal evolution and risk profiling of the COVID-19 epidemic in Shaanxi Province. *Tropical Geography*, 40(3), 432–445. (in Chinese)

Wells WF (1995). Airborne Contagion and Air Hygiene: An Ecological Study of Droplet Infection. Cambridge, MA, USA: Harvard University Press.

WHO (2020). Coronavirus Disease 2019 (COVID-19) Situation Report-30. Available at https://www.who.int/docs/default-source/coronaviruse/situation-reports/20200219-sitrep-30-covid-19.pdf?sfvrsn=3346b04f_2.

Wong MS, Nichol JE, To PH, et al. (2010). A simple method for designation of urban ventilation corridors and its application to urban heat island analysis. *Building and Environment*, 45: 1880–1889.

Wu Z, Li D (2011). Principles of Urban Planning, 4th Edn. Beijing: China Architecture & Building Press. (in Chinese)

Wu Z, Ye Z (2016). Research on urban spatial structure based on Baidu heat map: A case study on the central city of Shanghai. *City Planning Review*, 40(04): 33–40. (in Chinese)

Xie X, Li Y, Chwang ATY, et al. (2007). How far droplets can move in indoor environments—Revisiting the Wells evaporation–falling curve. *Indoor Air*, 17: 211–225.

Xu C, Nielsen PV, Liu L, et al. (2017). Human exhalation characterization with the aid of schlieren imaging technique. *Building and Environment*, 112: 190–199.

Xu C, Wei X, Liu L, et al. (2020). Effects of personalized ventilation interventions on airborne infection risk and transmission between occupants. *Building and Environment*, 180: 107008.

Yang J, Shi B, Shi Y, et al. (2020). Construction of a multi-scale spatial epidemic prevention system in high-density cities. *City Planning Review*, 44(03): 17–24. (in Chinese)

Zachreson C, Mitchell L, Lydeamore MJ, et al. (2021). Risk mapping for COVID-19 outbreaks in Australia using mobility data. *Journal of the Royal Society Interface*, 18: 20200657.

Zhang H, Zhu S, Wang M, et al. (2015). Sky view factor estimation based on 3D urban building data and its application in urban heat island—Illustrated by the case of Adelaide. *Remote Sensing Technology and Application*, 30(5): 899–907. (in Chinese)

Zhang Y, Feng G, Bi Y, et al. (2019). Distribution of droplet aerosols generated by mouth coughing and nose breathing in an air-conditioned room. *Sustainable Cities and Society*, 51: 101721.

Zhang Y, Wang X, Bi Q (2020). Travel-infected susceptibility based on transmission mechanism of COVID-19. *Transport Research*, 6(1): 73–80. (in Chinese)

Zhu S, Srebric J, Spengler JD, et al. (2012). An advanced numerical model for the assessment of airborne transmission of influenza in bus microenvironments. *Building and Environment*, 47: 67–75.